Applied Surface Science 505 (2020) 144218

Contents lists available at ScienceDirect

Applied Surface Science

journal homepage: www.elsevier.com/locate/apsusc

Full Length Article

Interaction of Ge with single layer GaAs: From Ge-island nucleation to formation of novel stable monolayers

Y. Sozen[a], I. Eren[b], S. Ozen[a], M. Yagmurcukardes[c,*], H. Sahin[a,d]

[a] Department of Photonics, Izmir Institute of Technology, 35430 Izmir, Turkey
[b] Department of Physics, Izmir Institute of Technology, 35430 Izmir, Turkey
[c] Department of Physics, University of Antwerp, Groenenborgerlaan 171, B-2020 Antwerp, Belgium
[d] ICTP-ECAR Eurasian Center for Advanced Research, Izmir Institute of Technology, 35430 Izmir, Turkey

ARTICLE INFO

Keywords:
Surface modification
Janus single-layers
DFT calculations
Vibrational properties
Elastic properties

ABSTRACT

In this study, reactivity of single-layer GaAs against Ge atoms is studied by means of *ab initio* density functional theory calculations. Firstly, it is shown that Ge atoms interact quite strongly with the GaAs layer which allows the formation of Ge islands while it hinders the growth of detached germanene monolayers. It is also predicted that adsorption of Ge atoms on GaAs single-layer lead to formation of two novel stable single-layer crystal structures, namely 1H-GaGeAs and $1H^A$-GaGeAs. Both the total energy optimizations and the calculated vibrational spectra indicate the dynamical stability of both single layer structures. Moreover, although both structures crystallize in 1H phase, 1H-GaGeAs and $1H^A$-GaGeAs exhibit distinctive vibrational features in their Raman spectra which is quite important for distinguishing the structures. In contrast to the semiconducting nature of single-layer GaAs, both polytypes of GaGeAs exhibit metallic behavior confirmed by the electronic band dispersions. Furthermore, the linear-elastic constants, in-plane stiffness and Poisson ratio, reveal the ultra-soft nature of the GaAs and GaGeAs structures and the rigidity of GaAs is found to be slightly enhanced via Ge adsorption. With their stable, ultra-thin and metallic properties, predicted single-layer GaGeAs structures can be promising candidates for nanoscale electronic and mechanical applications.

1. Introduction

Bulk GaAs, one of the important member of group III-V semiconductors, has been the most valid material in optoelectronics applications due to its advanced electronic properties such as highly efficient light emission [1] and high electron mobility [2]. For decades, it has been used in solar cell device technology [1,3,4], in light emitting diodes [5–7], in lasers [8–10], and in detectors [11,12].

For decades, doping has been used as a common technique for the manipulation of the electronic and optical properties of semiconductors in order to increase their performance in device applications [13–17]. The most widely studied dopants of GaAs are Si and C. It was reported that Si atoms are generally integrated as donors occupying the Ga sites and leading to *n*-type doped GaAs crystals [18,19] while C atoms were reported to act as acceptors occupying As sites and resulting in *p*-type doped GaAs [20,21]. In contrast, it was also announced that site selection of impurities can be manipulated by the adjustment of suitable conditions like growth temperature [22,23] and concentration level [24]. Besides, reported by Ohno et al., GaAs possess ferromagnetic properties by doping with Mn atom which has become one of the first sparks of the investigation of spin-based technologies [25]. Furthermore, several theoretical studies focused on the growth of nanostructures by the adsorption of adatoms on the surface of bulk GaAs crystal [26–29]. Very recently, Gutierrez-Ojeda et al., reported the adsorption characteristics and formation of monolayer/bilayers of Mn and Ge adatoms on GaAs (111) surface [28]. The study also concluded that the termination of GaAs surface with Mn atoms leads to an interface with antiferromagnetic distribution.

Moreover, advances in experimental techniques have also led to emergence of novel GaAs in low-dimensional forms. Single-layer form of GaAs was theoretically predicted to exhibit dynamically stable buckled honeycomb structure in its ground state [30]. It was shown that single-layer GaAs reaches its favorable energy state in low buckled configuration by the formation of unsteady bonds due to $s - p$ overlapping. Besides, Wu et al. investigated the electric field-dependent electronic and structural properties of single-layer GaAs [31]. In addition, Bahuguna et al. reported the insulator to metallic transition via increased electric field strength in single-layer GaAs [32]. Moreover,

* Corresponding author.
E-mail address: Mehmet.Yagmurcukardes@uantwerpen.be (M. Yagmurcukardes).

https://doi.org/10.1016/j.apsusc.2019.144218
Received 30 July 2019; Received in revised form 18 September 2019; Accepted 28 September 2019
Available online 31 October 2019
0169-4332/

Rozahun et al. reported that while the Ga vacancies lead to the non-magnetic-to-magnetic transition, As vacancies result in semimetallic-to-metallic transition in single-layer GaAs [33]. Very recently, Chung et al. constructed a generalized tight-binding model in order to fully explore the magneto-electronic properties of single-layer GaAs [34].

In this study, by predicting the strong interaction of Ga atoms with Ge atoms, we propose the formation of two different phases of GaGeAs, single-layers of Janus type 1H-GaGaAs and alloy $1H^A$-GaGeAs, by means of first-principles calculations. The electronic, vibrational, and linear-elastic properties of both structures are investigated and compared in order to understand their distinctive properties.

2. Computational methodology

First principle calculations in the basis of density functional theory were performed for the investigation of structural, vibrational, and electronic properties by using Vienna *ab initio* simulation package [35,36]. Augmented wave (PAW) [37] pseudopotential datasets were used, and the exchange-correlation functionals were adapted by generalized gradient approximation (GGA) that depends on the Perdew-Burke-Ernzerhof functionals (PBE) [38] with the inclusion of spin-orbit coupling (SOC). Due to the inefficiency of GGA functional defining the van der Waals type Coulomb interactions, DFT-D2 correction was used which has been derived by Grimme [39]. To find charge transition between atoms, bader technique was used which divides atoms into subsystems by constructing a bader volume using zero flux surface to obtain charge density on individual atoms [40].

The energy cutoff was taken to be 500 eV for plane wave basis set. A $24 \times 24 \times 1$ Γ centered *k*-point grids were used for the primitive unit cell optimizations of single-layer GaAs and 1H-GaGeAs while it was reduced to $12 \times 12 \times 1$ for the single-layer $1H^A$-GaGeAs. Self consistency loop was carried out until the total energy difference between two electronic step became 10^{-6} eV. Vacuum spacing was taken to be 15 Å to prevent possible Coulomb interactions between the repeating layers in the out-of-plane direction. The dipole moment correction was used for the workfunction calculations to suppress the effect of induced electric dipole moment. Cohesive energy per atom was calculated by the representative equation which is given as; $E_{Coh/atom} = E_G[XY] - n_X E_G[X] - n_Y E_G[Y]/n_{total}$ where E_G[XY] is the total ground state energy of the optimized structure, E_G[X] and E_G[Y] are the single atom energies, n_X and n_Y are the total number of each atomic species and n_{total} is the total number of atoms inside the unit cell. The binding energy of Ge atom on different adsorption sites was calculated with the formula; $E_{Ge-binding} = E_G[Ge + GaAs] - E_G[GaAs] - E_G[Ge]$ where E_G[Ge + GaAs] is the total ground state energy of Ge adsorbed GaAs single-layer, E_G[GaAs] and E_G[Ge] are the total ground state energies of bare GaAs monolayer and single Ge atom. The phonon modes both at the Γ point and the whole Brillouin zone were calculated by using the small displacement method as implemented in the PHON code, and the corresponding off-resonant Raman activities were obtained from the derivative of dielectric constant using finite-difference method [41].

3. From single Ge adsorption to Ge-encapsulation

In this section, we present our results for the adsorption characteristics of Ge atom on single-layer GaAs. Due to the buckled structure of GaAs, the adsorption of Ge atom on each atomic plane is considered, separately. Totally eight different adsorption sites (four on each plane), which are defined as; the hollow site of a single honeycomb (As_H and Ga_H), on top of the Ga atom (Ga_D and Ga_T), on top of the As atom (As_T and As_D) and on top of the center of Ga-As bond (As_B and Ga_B), are considered (see Fig. 1). To avoid the neighboring interactions between repeated Ge atoms, adsorption calculations are performed on $4 \times 4 \times 1$ supercell.

Our results reveal that Ge atom strongly interacts with GaAs layer on all sites. The energetically most favorable site is found to be the Ga_D site with a binding energy of 3.71 eV. In addition, the strong interaction of Ge atom on Ga_D site results in the distortion of Ga atom through the out-of-plane direction. As an alternative adsorption site (binding energy of 2.62 eV), As_T is found to cause the formation of dumbbell shaped Janus type GaGeAs unit by pushing out the As atom towards out-of-plane direction. Ge atom diffusing through the atomic plane of Ga favors to bind on Ga_T site with a binding energy of 2.89 eV by pulling out the Ga atom from its atomic plane. Notably, on the bridge sites, Ge atom does not prefer to be adsorbed since it prefers to diffuse along the As atom. As in the case of As_T, Ge adsorption on As_D site causes the formation of dumbbell shaped GaGeAs unit.

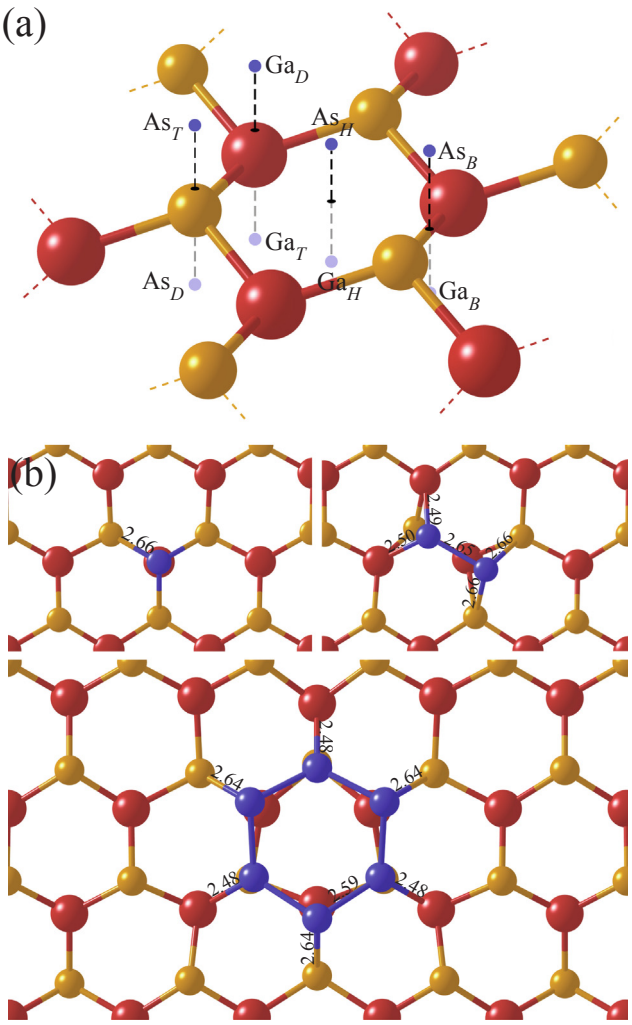

Fig. 1. (a) Possible adsorption sites for Ge atom on each atomic plane of single-layer GaAs. (b) Illustration of the growth of hexagonal Ge_N clusters (N = 2,6) starting from the single Ge adsorption on favorable Ga_D site. The atomic bond lengths are given on each corresponding bond. Blue, red, and orange colors represent Ge, Ga and As atoms, respectively.

Following the analysis of single Ge adsorption, the formation of Ge hexagonal ring on the single-layer GaAs is investigated through the binding energies of various adsorption sites. Energetically the most favorable site is found to be the top of Ga atoms which strongly interact with Ge atoms. It is expected that the Ge adatoms bind to Ga_D and the Ga_T atoms. After the occupation of Ga sites with Ge atoms that results in structural distortions in the crystal, the As sites (both the top and down As atoms) are occupied by Ge atoms due to considerably high binding energies. As shown in the bottom panel of Fig. 1, Ge atoms diffuse onto GaAs single-layer and adsorbed at Ga_D site and the second Ge atom is binded to As_T site resulting in the formation of Ge_2 dimer. The process is

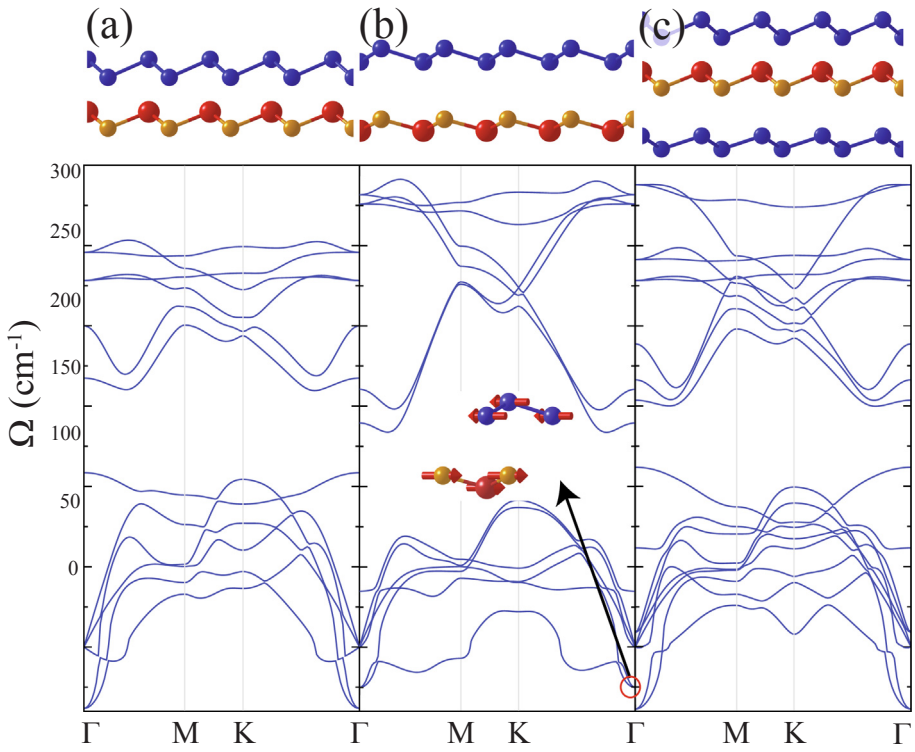

Fig. 2. (a) and (b) Calculated phonon dispersion curves for single-layer germanene on Ga plane and As plane for two possible stackings. (c) That of single-layer GaAs encapsulated between germenene layers.

carried out until the formation of Ge_6 ring in hexagonal configuration occurs. Since the atomic mass and radius of Ge is in between those of Ga and As, the formed hexagonal Ge_6 ring have slightly distorted shape. It is evident that the formation of hexagonal Ge_6 ring on top of the GaAs can lead to the formation of GeGaAs single-layer crystal.

As shown in Fig. 1b, as the number of adsorbed Ge atoms increase, due to strong interaction of Ge atoms each other, the formation of Ge-hexagons seems to be feasible which may allow also the formation of a single-layer structure composed of purely Ge atoms, namely germanene. Therefore, it is important to consider the possible scenarios in which the GaAs layer is covered by single-layer germanene or it is encapsulated by germanene layers. The bilayer structures of GaAs and germanene layers can be formed in two different stackings (see Fig. 1b, and for both coverage the encapsulated GaAs layer is constructed (see Fig. 2c).

Structural optimizations reveal that the interaction of germanene with GaAs single-layer vary depending on the atomic plane that its coupled. When germanene layer on Ga plane (see Figs. 2a), Ge atoms reside closer to As atom. Due to the small distance between closest atoms, it is expected that the attraction between layers are different from a typical vdW type heterostructures such that the binding energy is calculated to be 205 meV/atom indicating the strong interaction between the layers. In contrast, when the lower Ge atom resides on As atom (see Figs. 2b), the layer-layer binding energy is found to be a 51 meV/atom which is much smaller than the other stacking. However, even the latter binding energy between the layers is higher as compared to heterostructures of well-known single-layers such as TMDs (33 meV/atom for MoS_2/WS_2) [42]. In contrast, germanene based heterostructures were reported to exhibit high binding energies than a typical vdW type heterostructures (95 meV/atom in Ge/InSe heterostructure) [43]. In the encapsulated structure, the interlayer distances are not symmetric with respect to the GaAs layer due to the difference interaction on each atomic plane. Accordingly, phonon band dispersions for all three stacking configurations reveal that two dynamically stable single-layers, germanene and GaAs, form dynamically unstable heterostructures in all three configurations which is not the case in typical dynamically stable vdW type heterostructures. As shown in the inset of Fig. 2b, the phonon instability in Germanene/GaAs heterostructures arise from the in-plane shear vibration of the layers against each other.

4. Formation of GaGeAs structures

As a consequence of the strong interaction of Ge atoms on GaAs single-layer, we consider the formation GaGeAs polytypes. It is found that two different polytype can be constructed, namely Janus type 1H-GaGeAs and alloy $1H^A$-GaGeAs. Janus type 1H-GaGeAs structure is formed upon the coverage of As_D sites (see Fig. 3a) while alloy $1H^A$-GaGeAs is constructed by the chemisorption of Ge atoms alternatingly on As_D and As_T sites of GaAs layer (see Fig. 3a). As listed in Table 1, the lattice parameters ($a = b$) of the optimized hexagonal GaGeAs structures are found to be 3.81 and 7.64 Å for 1H-GaGeAs and $1H^A$-GaGeAs, respectively. Notably, the repeating unit of the single-layer $1H^A$-GaGeAs is constructed in a $2 \times 2 \times 1$ super cell so that the lattice parameter of 1H-GeGaAs is slightly smaller (0.02 Å). The bond lengths between Ga-As/Ga-Ge atoms are calculated to be 2.67/2.50 Å and 2.65/2.52 Å in 1H-GaGeAs and $1H^A$-GaGeAs, respectively. In addition, the cohesive energies per atom are listed in Table 1 and it is indicated that the construction of Janus type 1H-GaGeAs is energetically more favorable over $1H^A$-GaGeAs. Moreover, according to Bader charge analysis Ge and Ga atoms donate 0.1 e and 0.3 e to each As atom, respectively in both structures that the anisotropic charge distribution induces an out-of-plane polarization in the Janus type 1H-GaGeAs. Furthermore, the work functions (Φ) from both atomic plane are calculated and listed in Table 1. The single-layer 1H-GaGeAs is found to exhibit 4.27 and 3.88 eV of work function calculated from As and Ge sites while $1H^A$-GaGeAs possesses 4.10 eV. The Ge site in 1H-GaGeAs has the lowest Φ indicating the tendency of the site to the chemical functionalization.

After the validity of the computational methodology is examined

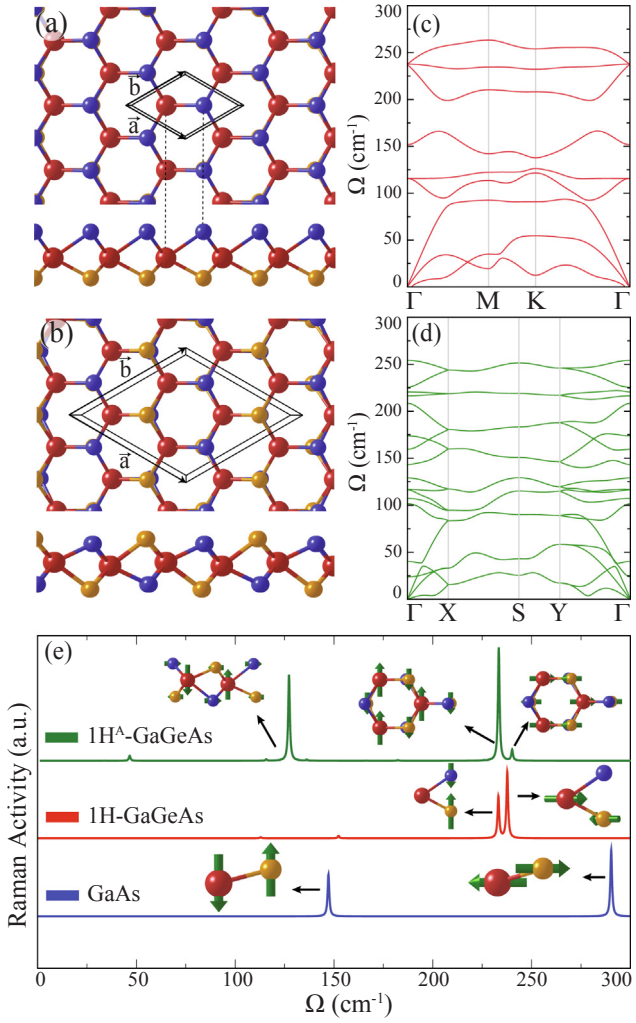

Fig. 3. The top and side views of single-layer (a) 1H-GaGeAs and (b) $1H^A$-GaGeAs. (c) and (d) The corresponding phonon band dispersions, respectively. (e) Raman spectrum of each GaGeAs structures and that of single-layer GaAs for comparison. The vibrational characteristics of some prominent Raman active modes are shown in the inset.

through the bulk GaAs (see Fig. S1), the dynamical stability of each GaGeAs structure is investigated in terms of the phonon band dispersions through the whole BZ. As shown in Fig. 3, single-layer GaGeAs crystals are free from any imaginary frequencies in the whole BZ. Both structures exhibit six optical phonon branches, two of which are non-degenerate and are attributed to the out-of-plane vibration of the individual atoms, four of which arise from two doubly-degenerate in-plane vibrations of the constituent atoms.

Later on the verified dynamical stability of each GaGeAs structure, the first-order Raman spectrum of each structure is investigated in terms of the Raman activity of each phonon mode. Notably, Raman spectrum of single-layer GaAs is also calculated for comparison. In its buckled structure, single-layer GaAs possesses two Raman active modes, one non-degenerate A-peak arising from the out-of-plane vibration of Ga and As atoms against each other and a doubly-degenerate (E-peak) which is attributed to the in-plane vibration of the atoms. The E-peak is found to be at frequency of 290.3 cm^{-1} while the A-peak is found to have frequency of 147.2 cm^{-1}.

In its 1H phase, single-layer Janus type GaGeAs exhibits totally different Raman spectrum than that of single-layer GaAs. Due to the out-of-plane anisotropy in 1H-GaGeAs, all of the six optical modes are found to be Raman active. The in-plane doubly-degenerate Raman active modes are found to have frequencies of 237.7 and 112.9 cm^{-1}, respectively. The out-of-plane vibrational mode having frequency 233.2 cm^{-1} is attributed to the opposite vibration of Ge and As atoms against each other (see inset in Fig. 3(e)). The other out-of-plane Raman active mode is calculated to have frequency of 152.3 cm^{-1} arising from the opposite vibration of Ga atom against Ge-As atoms. Raman activity analyses reveal that the most prominent active mode is found to be E_g-like mode (at 237.7 cm^{-1}) while the A_g-like mode (at 233.2 cm^{-1}) is calculated to have Raman activity which is half of that for E_g-like mode. The other in-plane and out-of-plane Raman active modes are calculated to possess activities which are approximately 50 times smaller than that of the prominent peak.

As shown in Raman spectrum of single-layer $1H^A$-GaGeAs, its structure possesses two prominent Raman active modes whose frequencies are calculated to be 231.2 and 121.4 cm^{-1}, respectively. Apart from the prominent peaks, a Raman active mode having frequency 238.2 cm^{-1} is found to exist with a relatively smaller activity (almost 10 times smaller than that of the mode at 232.2 cm^{-1}) (see Fig. 3e). The phonon mode at 238.2 cm^{-1} is characterized by the in-plane vibration of Ga and As atoms against each other along the armchair direction while the mode at 231.2 cm^{-1} is attributed to the same type of vibration along the zigzag direction. It is seen that the degeneracy of the two in-plane modes is broken due to exchange of As atoms with Ge atoms. In addition, the phonon mode at 121.4 cm^{-1} arises from the opposite out-of-plane vibation of Ga atoms while Ge and As atoms have smaller opposite in-plane vibrational contribution. It is seen that the GaGeAs structures display distinctive vibrational features so that the phases are distinguishable in terms of their Raman spectra.

Electronic properties of single-layer GaAs and GaGeAs structures are investigated in terms of their electronic band dispersions and partial density of states (PDOS) and those for GaGeAs structures as presented in Fig. 4. Single-layer GaAs is calculated as direct band gap semiconductor whose valence band maximum (VBM) and conduction band minimum (CBM) reside at the Γ symmetry point (Fig. S2(a)). It is seen that, the inclusion of SOC dramatically effects the splitting near the valence band edge which also indicates the indirect or direct band gap behavior of the single-layer GaAs. The VBM band edge is found to be dominated by the mixing of p_x-p_y orbitals of both As and Ga atoms while the CBM edge is dominated by the Ga-*s* and As-*s* orbitals (Fig. S2(b) and Fig. S3(a)).

In contrast to single-layer GaAs, the presence of the electronic states in the vicinity of Fermi level indicate the metallic nature of Janus 1H-GaGeAs and alloy $1H^A$-GaGeAs single-layers. The band splittings at the

Table 1
For the single-layer structures of GaAs, 1H-GaGeAs, and $1H^A$-GaGeAs crystals; the optimized lattice constants, $a = b$; bond lengths between the individual atoms, d_{X-Y}; the thickness of the structure, t; total magnetic moment, μ; total amount of electron donated (-) or received (+) by the atom, ρ_{Ga}, ρ_{Ge} and ρ_{As}; cohesive energy per atom, E_{Coh}, workfunction, Φ, the in-plane stiffness, C, and Poisson ratio, ν.

	$a = b$ (Å)	d_{Ga-Ge} (Å)	d_{Ga-As} (Å)	t (Å)	μ (μ_B)	ρ_{Ga} (e^-)	ρ_{Ge} (e^-)	ρ_{As} (e^-)	E_{Coh} (eV)	Φ (eV)	C (N/m)	ν (–)
GaAs	4.01	–	2.40	0.62	0	−0.6	–	+0.6	2.91	4.55(Ga) 5.38(As)	43	0.35
1H-GaGeAs	3.81	2.67	2.50	2.70	0	−0.3	−0.1	+0.4	3.16	4.27(As) 3.88(Ge)	48	0.45
$1H^A$-GaGeAs	7.64	2.65	2.52	2.69	0	−0.3	−0.1	+0.4	3.13	4.10	55	0.37

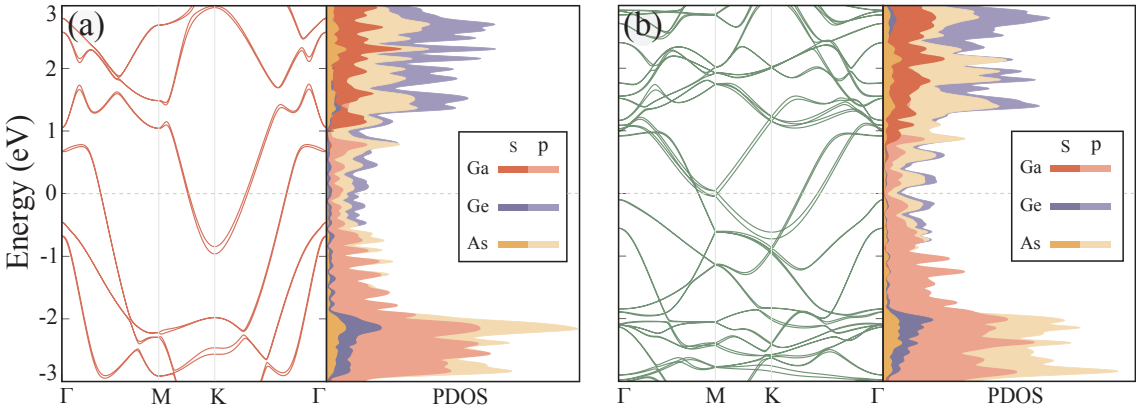

Fig. 4. Calculated electronic band diagrams and partial density of states (PDOS) of (a) 1H-GaGeAs and (b) 1H^A-GaGeAs. Dashed line at 0 eV represents the Fermi level.

K point indicate the significant spin-orbit interaction in Janus 1H-GaGeAs. In lowest conduction band edge, such splitting is calculated to be approximately 116 meV. Similarly, the spin-orbit splitting reside around the Fermi level and expands to upper states in alloy 1H^A-GaGeAs.

For GaGeAs polytypes, we further analyze the orbital characters of the energy bands crossing the Fermi level either at or between the high symmetry points (Fig. S3(b) and S3(c)). In single-layer Janus 1H-GaGeAs, at three different points (between the Γ-M, M-K, and K-Γ, respectively) the bands are found to cross the Fermi level. For the bands crossing at the Γ-M and K-Γ *s*-orbital of As atoms and mixed *s-p* orbitals of Ge atoms have contributions. On the other hand, the band crossing between the M-K is mostly contributed by the purely p_x and p_y orbitals of As atoms and mixed *s-p* orbitals of Ge atoms. In the case of single-layer alloy 1H^A-GaGeAs, the contributions of the atomic orbitals are found to be symmetric on both atomic plane. The bands crossing the Fermi level in between the Γ-M are found to be dominated by the shared *p*-orbitals of Ga-As and Ga-Ge bonds, respectively. However, the orbital characters of the bands crossing at the K-Γ are calculated to be localized on p_x and p_y orbitals of Ge and As atoms, respectively.

The elastic properties of single-layer GaAs and GaGeAs structures are also investigated through linear-elastic constants, namely in-plane stiffness (C) and the Poisson ratio (ν). In order to determine the linear-elastic constants, the elastic strain tensor elements, C_{ij}, are calculated and the corresponding C and ν values are obtained in for two main orientations of the lattice, zigzag and armchair directions. As listed in Table 1, both of the C and ν are calculated to be same for armchair (AC) and zigzag (ZZ) orientations of the lattice in three single-layers. In addition, the orientation angle-dependent linear-elastic constants are also calculated by using the functions given below [44,45];

$$C(\theta) = \frac{(C_{11}C_{22} - C_{12}^2)}{C_{22}cos^4(\theta) + Acos^2(\theta)sin^2(\theta) + C_{11}sin^4(\theta)} \quad (1)$$

$$\nu(\theta) = \frac{C_{12}cos^4(\theta) - Bcos^2(\theta)sin^2(\theta) + C_{12}sin^4(\theta)}{C_{22}cos^4(\theta) + Acos^2(\theta)sin^2(\theta) + C_{11}sin^4(\theta)} \quad (2)$$

where the numbers A and B are defined as; $A = (C_{11}C_{22} - C_{12}^2)/C_{66} - 2C_{12}$ and $B = C_{11} + C_{22} - (C_{11}C_{22} - C_{12}^2)/C_{66}$.

The in-plane stiffness, the measure of the rigidity of a material, is calculated to increase as the Ge atoms are adsorbed on single-layer GaAs. In-plane stiffness of GaAs is found to be 43 N/m (slightly smaller than that of reported by Sahin et al., 48 N/m) [30] while in single-layer Janus GaGeAs it increases to 48 N/m and it reaches to 55 N/m in alloy single-layer 1H^A-GaGeAs. The calculated values indicate the soft nature of the all three single-layers that arise from the relatively weak Ga-As and Ga-Ge bonds in the structures. In addition as shown by Fig. 5a, single-layer alloy GaGeAs possesses in-plane anisotropy around the orientation angle of 45°. This occurs due to the non-uniform distribution of As and Ge atoms. The same anisotropy is not found in Janus GaGeAs because the structure exhibits the anisotropy between two outer planes while the in-plane atomic distribution is uniform on two outer planes, respectively. Among 2D ultra-thin materials, graphene is known to be the stiffest material with a large in-plane stiffness (330 N/m) [46] as a result of the strong in-plane C-C bonds. Due to different type of atomic arrangement of the atoms, single-layer MoS_2 is known to be slightly softer than graphene (with a stiffness of 122 N/m) [46]. In addition, as compared to the in-plane stiffness of monoatomic single-layer of Germanene (48 N/m) [30], single-layers of 1H- and 1H^A-GaGeAs exhibit quiet similar elastic properties.

Poisson ratio, the ratio of the transverse contraction strain to the longitudinal extension, is calculated for each single-layer and is listed in Table 1. The Poisson ratio for single-layer 1H^A-GaGeAs (0.37) is found to be close to that of GaAs (0.35) while single-layer 1H-GaGeAs exhibits relatively larger value (0.45). Notably, alloy single-layer GaGeAs, 1H^A-GaGeAs, possesses similar Poisson ratio with that of single-layer GaAs due to the homogeneous distribution of Ge and As atoms along AC and ZZ directions. However, in single-layer Janus 1H-GaGeAs, fully different outer lattice planes experience compressive and tensile strain, respectively that a small bending occurs in the structure. Therefore, its relatively higher Poisson ratio indicates the strong ability of single-layer Janus 1H-GaGeAs to preserve its equilibrium state under external applied strain. On the other hand, alloy GeGaAs is found to exhibit in-plane anisotropy as shown in Fig. 5b. It is seen that around 45° of the orientation angle, alloy GaGeAs possesses slightly larger Poisson ratio than that of the Janus structure. Consequently, the soft nature of GaAs and GaGeAs structures results in relatively larger Poisson ratio as compared to well-known single-layer materials (0.20 for graphene and 0.26 MoS_2) [46].

5. Conclusions

In this study, by investigating the interaction mechanism of Ge atoms on single-layer GaAs, the formation of possible single-layer GaGeAs structures were predicted in the framework of density functional theory-based *ab initio* calculations. Total energy calculations revealed that Ge atoms interact quite strongly with the GaAs layer allowing the formation of Ge rings while the growth of detached germanene monolayers on the GaAs is hindered (revealed by the dynamical instability of the germanene/GaAs heterostructures). In addition, it was shown that selective adsorption of Ge atoms on possible sites on GaAs lead to the formation of two novel single-layers, namely 1H-GaGeAs and 1H^A-GaGeAs. The total energy optimizations, structural relaxations, and the phonon band dispersions indicated the dynamical stability of both GaGeAs structures. Moreover, although both structures possess 1H phase, 1H-GaGeAs and 1H^A-GaGeAs were shown to exhibit

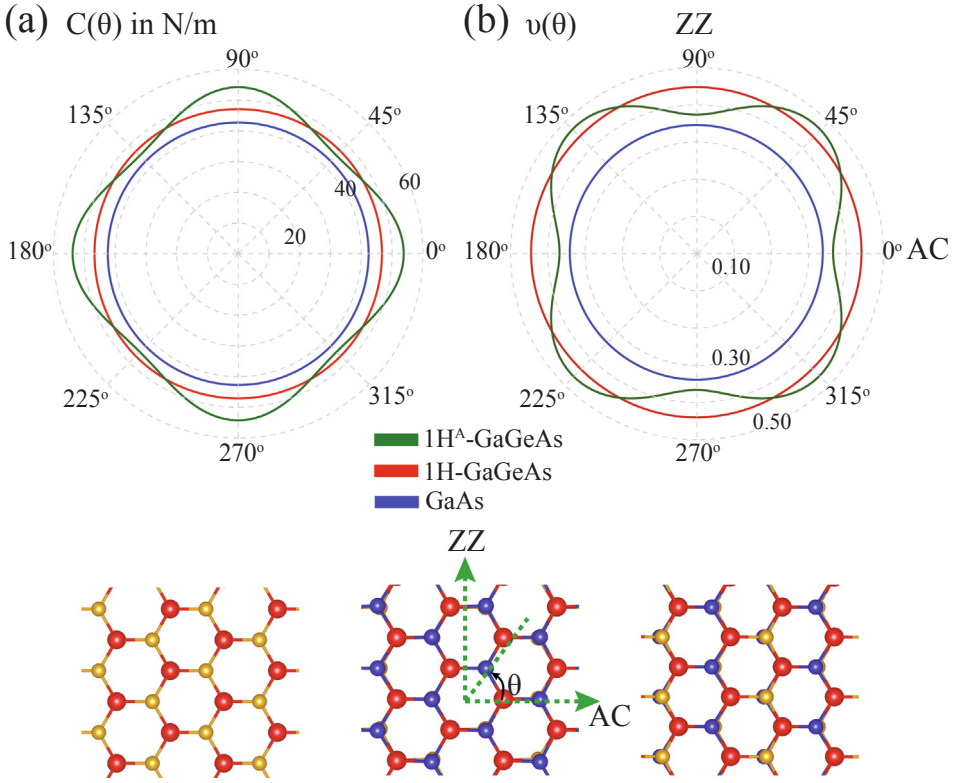

Fig. 5. For the single-layers of GaAs, 1H-GaGeAs, and 1H^A-GaGeAs crystals the orientation angle-dependent; (a) in-plane stiffness, C(θ) and (b) Poisson ratio, $\nu(\theta)$. AC and ZZ stand for the armchair and zigzag directions, respectively in all structures.

distinctive vibrational features in their Raman spectrum which is quite important for distinguishing the structures. Electronic band structure calculations revealed that in contrast to the semiconducting nature of single-layer GaAS, both polytypes of GaGeAs structure exhibit metallic behavior. Furthermore, the linear-elastic constants, in-plane stiffness and Poisson ratio, indicated the ultra-soft nature of the GaAs and GaGeAs single-layers. Overall, our findings revealed that the formation of dynamically sTable 1H-GaGeAs and 1H^A-GaGeAs structures seems feasible via the adaptation of Ge atoms into GaAs layer rather than the formation of Germanene/GaAs heterostructures.

Declaration of Competing Interest

The authors declared that there is no conflict of interest.

Acknowledgments

Computational resources were provided by TUBITAK ULAKBIM, High Performance and Grid Computing Center (TR-Grid e-Infrastructure). H.S. acknowledges financial support from the Scientific and Technological Research Council of Turkey (TUBITAK) under the project number 117F095. H.S. acknowledges support from Turkish Academy of Sciences under the GEBIP program. This work is supported by the Flemish Science Foundation (FWO-Vl) by a postdoctoral fellowship (M.Y.).

Appendix A. Supplementary material

Supplementary data associated with this article can be found, in the online version, at https://doi.org/10.1016/j.apsusc.2019.144218.

References

[1] E.D. Kosten, J.H. Atwater, J. Parsons, A. Polman, H.A. Atwater, Light: Sci. Appl. 2 (2013) e45.
[2] C.M. Wolfe, G.E. Stillman, W.T. Lindley, J. Appl. Phys. 41 (1970) 3088.
[3] H. Ehrenreich, Phys. Rev. 120 (1960) 1951.
[4] G. Mariani, A.C. Scofield, C.-H. Hung, D.L. Huffaker, Nat. Commun. 4 (2013) 1497.
[5] H.J. Zhu, M. Ramsteiner, H. Kostial, M. Wassermeier, H.-P. Schönherr, K.H. Ploog, Phys. Rev. Lett. 87 (2001) 016601.
[6] R. Fiederling, M. Keim, G. Reuscher, W. Ossau, G. Schmidt, A. Waag, L.W. Molenkamp, Nature 402 (1999) 787–790.
[7] S.I. Tsintzos, N.T. Pelekanos, G. Konstantinidis, Z. Hatzopoulos, P.G. Savvidis, Nature 453 (2008) 372–375.
[8] H. Liu, T. Wang, Q. Jiang, R. Hogg, F. Tutu, F. Pozzi, A. Seeds, Nat. Phot. 5 (2011) 416–419.
[9] B. Mayer, D. Rudolph, J. Schnell, S. Morktter, J. Winnerl, J. Treu, K. Müller, G. Bracher, G. Abstreiter, G. Koblmüller, J.J. Finley, Nat. Commun. 4 (2013) 2931.
[10] D. Saxena, S. Mokkapati, P. Parkinson, N. Jiang, Q. Gao, H.H. Tan, C. Jagadish, Nat. Phot. 7 (2013) 963–968.
[11] X. Dai, S. Zhang, Z. Wang, G. Adamo, H. Liu, Y. Huang, C. Couteau, C. Soci, Nano Lett. 14 (2014) 2688–2693.
[12] K. Peng, P. Parkinson, L. Fu, Q. Gao, N. Jiang, Y.-N. Guo, F. Wang, H.J. Joyce, J.L. Boland, H.H. Tan, C. Jagadish, M.B. Johnston, Nano Lett. 15 (2015) 206–210.
[13] D. Olego, M. Cardona, H. Müller, Phys. Rev. B 22 (1980) 894.
[14] D. Olego, M. Cardona, Phys. Rev. B 22 (1980) 886.
[15] H.C. Casey, F. Stern, J. Appl. Phys. 47 (1976) 631.
[16] M.I. Nathan, W.P. Dumke, K. Wrenner, S. Tiwari, S.L. Wright, K.A. Jenkins, Appl. Phys. Lett. 52 (1988) 654.
[17] T. Burgess, D. Saxena, S. Mokkapati, Z. Li, C.R. Hall, J.A. Davis, Y. Wang, L.M. Smith, L. Fu, P. Caroff, H.H. Tan, C. Jagadish, Nat. Commun. 7 (2016) 11927.
[18] M.D. Pashley, K.W. Haberern, Phys. Rev. Lett. 67 (1991) 19.
[19] C. Lee, N. Lee, K. Lee, J. Kim, H. Park, D. Kwak, H.C. Lee, H. Lim, J. Appl. Phys. 77 (1995) 6727.
[20] N. Kobayashi, T. Makimoto, Y. Horikoshi, Appl. Phys. Lett. 50 (1987) 1435.
[21] S.A. Stockman, G.E. Höfler, J.N. Baillargeon, K.C. Hsieh, K.Y. Cheng, G.E. Stillman, J. Appl. Phys. 72 (1992) 981.
[22] H. Rupprecht, J.M. Woodall, K. Konnerth, D.G. Pettit, Appl. Phys. Lett. 9 (1966) 221.
[23] W.Y. Lum, H.H. Wieder, J. Appl. Phys. 49 (1978) 6187.
[24] C. Domke, Ph. Ebert, M. Heinrich, K. Urban, Phys. Rev. B 54 (1996) 10288.
[25] H. Ohno, A. Shen, F. Matsukura, A. Oiwa, A. Endo, S. Katsumoto, Y. Iye, Appl. Phys. Lett. 69 (1996) 363.
[26] S.J. Gutierrez-Ojeda, R. Garcia-Diaz, F. Sanchez-Ochoa, J. Guerrero-Sanchez, L.M. de la Garza, J. Varalda, D.H. Mosca, G.H. Cocoletzi, Appl. Surf. Sci. 455 (2018) 1078.
[27] R. Ponce-Prez, M.T.R. de la Cruz, S.J. Gutirrez-Ojeda, J. Guerrero-Snchez, J. Varalda, G.H. Cocoletzi, Appl. Surf. Sci. 489 (2019) 639.

[28] S.J. Gutierrez-Ojeda, J. Guerrero-Sanchez, R. Ponce-Preza, J. Varalda, D.H. Mosca, L.M. de la Garza, G.H. Cocoletzi, Appl. Surf. Sci. 491 (2019) 147.
[29] J. Guerrero-Snchez, J. Castro-Medina, J.F. Rivas-Silva, N. Takeuchi, L.M. de la Garza, J. Varalda, D.H. Mosca, G.H. Cocoletzi, Z. Phys. Chem. 230 (2016) 943.
[30] H. Sahin, S. Cahangirov, M. Topsakal, E. Bekaroglu, E. Akturk, R.T. Senger, S. Ciraci, Phys. Rev. B 80 (2009) 155453.
[31] J. Wu, Y. Yang, H. Gao, Y. Qi, J. Zhang, Z. Qiao, W. Ren, AIP Adv. 7 (2017) 035218.
[32] B.P. Bahuguna, L.K. Saini, B. Tiwaria, R.O. Sharmaa, RSC Adv. 6 (2016) 52920.
[33] I. Rozahun, T. Bahti, G. He, Y. Ghupur, A. Ablat, M. Mamat, Appl. Surf Sci. 441 (2018) 401–407.
[34] H.-C. Chung, C.-W. Chiu, M.-F. Lin, Sci. Rep. 9 (2019) 2332.
[35] G. Kresse, J. Hafner, Phys. Rev. B 47 (1993) 558.
[36] G. Kresse, J. Furthmüller, Phys. Rev. B 54 (1996) 11169.
[37] P. Blochl, Phys. Rev. B 50 (1994) 17953.
[38] J.P. Perdew, K. Burke, M. Ernzerhof, Phys. Rev. Lett. 77 (1996) 3865.
[39] S. Grimme, J. Comp. Chem. 27 (2006) 1787.
[40] G. Henkelman, A. Arnaldsson, H. Jonsson, Comput. Mater. Sci. 36 (2006) 354.
[41] D. Alf, Comput. Phys. Commun. 180 (2009) 2622–2633.
[42] B. Amin, N. Singh, U. Schwingenschlogl, Phys. Rev. B 92 (2015) 075439.
[43] Y. Fan, X. Liu, J. Wang, H. Aib, M. Zhao, Phys. Chem. Chem. Phys. 20 (2018) 11369.
[44] Y. Ma, L. Kou, B. Huang, Y. Dai, T. Heine, Phys. Rev. B 98 (2018) 085420.
[45] E. Cadelano, P.L. Palla, S. Giordano, L. Colombo, Phys. Rev. B 82 (2010) 235414.
[46] M. Yagmurcukardes, R.T. Senger, F.M. Peeters, H. Sahin, Phys. Rev. B 94 (2016) 245407.